

Learning Representations for Control with Hierarchical Forward Models

Trevor McInroe

University of Edinburgh
t.mcinroe@ac.ed.uk

Lukas Schäfer

University of Edinburgh
l.schaefer@ed.ac.uk

Stefano V. Albrecht

University of Edinburgh
s.ablrecht@ed.ac.uk

Abstract: Learning control from pixels is difficult for reinforcement learning (RL) agents because representation learning and policy learning are intertwined. Previous approaches remedy this issue with auxiliary representation learning tasks, but they either do not consider the temporal aspect of the problem or only consider single-step transitions. Instead, we propose Hierarchical k -Step Latent (HKSL), an auxiliary task that learns representations via a hierarchy of forward models that operate at varying magnitudes of step skipping while also learning to communicate between levels in the hierarchy. We evaluate HKSL in a suite of 30 robotic control tasks and find that HKSL either reaches higher episodic returns or converges to maximum performance more quickly than several current baselines. Also, we find that levels in HKSL’s hierarchy can learn to specialize in long- or short-term consequences of agent actions, thereby providing the downstream control policy with more informative representations. Finally, we determine that communication channels between hierarchy levels organize information based on both sides of the communication process, which improves sample efficiency.

Keywords: Reinforcement learning, Representation learning, Continuous control

1 Introduction

Recently, reinforcement learning (RL) has had significant empirical success in the robotics domain [1, 2, 3, 4]. However, previous methods often require a dataset of hundreds of thousands or millions of agent-environment interactions to achieve their performance. This level of data collection may not be feasible for the average industry group. Therefore, RL’s widespread real-world adoption requires agents to learn a satisfactory control policy in the smallest number of agent-environment interactions possible.

Pixel-based state spaces increase the sample efficiency challenge because the RL algorithm is required to learn a useful representation and a control policy simultaneously. A recent thread of research has focused on developing auxiliary learning tasks to address this dual-objective learning problem. These approaches aim to learn a compressed representation of the high-dimensional state space upon which agents learn control. Several task types have been proposed such as image reconstruction [5, 6], contrastive objectives [7, 8], image augmentation [9, 10], and forward models [11, 12, 13, 14, 15].

Forward models are a natural fit for RL because they exploit the temporal axis by generating representations of the state space that capture information relevant to the environment’s transition dynamics. However, previous approaches learn representations by predicting single-step transitions, which may not capture relevant information efficiently if important environmental changes take many steps to manifest. For example, if we wish to train a soccer-playing agent to score a goal, the pertinent portions of an episode occur at the beginning, when the agent applies a force and direction, and at the end when the agent sees how close the ball came to the goal. Skipping the large portion of the trajectory where the ball is rolling could lead to more efficient learning.

In this paper, we introduce *Hierarchical k -Step Latent* (HKSL)[†], an auxiliary task for RL agents that explicitly captures information in the environment at varying levels of temporal coarseness. HKSL

[†]<https://github.com/trevormcinroe/hksl>

accomplishes this by leveraging a hierarchical latent forward model where each level in the hierarchy predicts transitions with a varying number of steps skipped. Levels that skip more steps should capture a coarser understanding of the environment by focusing on changes that take more steps to manifest and vice versa for levels that skip fewer steps. HKSL also learns to share information between levels via a communication module that passes information from higher to lower levels. As a result, HKSL learns a set of representations that give the downstream RL algorithm information on both short- and long-term changes in the environment.

We evaluate HKSL and various baselines in a suite of 30 continuous-control environments [16, 17] that contains environments without and with distractors of varying types and intensities. We test our algorithms with and without distractors because real-world RL-controlled robots need to work well in controlled settings like a laboratory and uncontrolled settings like a public street. Also, distractors may change at speeds independently from task-relevant information, thereby increasing the challenge of relating agent actions to changes in pixels. Therefore, real-world RL deployments should explicitly learn representations that tie agent actions to long- and short-term changes in the environment. The goal in our study is to learn a well-performing control policy in the smallest number of agent-environment interactions as possible.

Our experiments show that HKSL significantly outperforms current baselines in terms of episodic returns in our evaluation suite. We analyze HKSL’s hierarchical model and find that representations can learn to specialize in varying levels of temporal coarseness, thereby providing the downstream control policy with more informative representations. Additionally, we find that HKSL’s communication manager considers both sides of the communication process, thereby giving forward models information that better contextualizes their learning process. Finally, we provide data from all training runs for all benchmarked methods.

2 Background

We study an RL formulation wherein an agent learns a control policy within a partially observable Markov decision process (POMDP) [18, 19], defined by the tuple $(\mathcal{S}, \mathcal{O}, \mathcal{A}, P^s, P^o, \mathcal{R}, \gamma)$. \mathcal{S} is the ground-truth state space, \mathcal{O} is a pixel-based observation space, \mathcal{A} is the action space, $P^s : \mathcal{S} \times \mathcal{A} \times \mathcal{S} \rightarrow [0, 1]$ is the state transition probability function, $P^o : \mathcal{S} \times \mathcal{A} \times \mathcal{O} \rightarrow [0, 1]$ is the observation probability function, $\mathcal{R} : \mathcal{S} \times \mathcal{A} \rightarrow \mathbb{R}$ is the reward function that maps states and actions to a scalar signal, and $\gamma \in [0, 1)$ is a discount factor. The agent does not directly observe the state $s_t \in \mathcal{S}$ at step t , but instead receives an observation $o_t \in \mathcal{O}$ which we specify as a stack of the last three images. At each step t , the agent samples an action $a_t \in \mathcal{A}$ with probability given by its control policy which is conditioned on the observation at time t , $\pi(a_t|o_t)$. Given the action, the agent receives a reward $r_t = \mathcal{R}(s_t, a_t)$, the POMDP transitions into a next state $s_{t+1} \in \mathcal{S}$ with probability $P^s(s_t, a_t, s_{t+1})$, and the next observation (stack of pixels) $o_{t+1} \in \mathcal{O}$ is sampled with probability $P^o(s_{t+1}, a_t, o_{t+1})$. Within this POMDP, the agent must learn a control policy that maximizes the sum of discounted returns over the time horizon T of the POMDP’s episode: $\arg \max_{\pi} \mathbb{E}_{a \sim \pi} [\sum_{t=1}^T \gamma^t r_t]$.

3 Related Work

Representation learning in RL. Some research has pinpointed the development of representation learning methods that can aid policy learning for RL agents. In model-free RL, using representation learning objectives as auxiliary tasks has been explored in ways such as contrastive objectives [7, 8], image augmentation [9, 10], image reconstruction [5], information theoretic objectives [20], and inverse models [21, 22]. HKSL fits within the auxiliary task literature but does not use contrastive objectives, image reconstruction, information theoretic objectives, nor inverse models.

Forward models and hierarchical models. Forward models for model-free RL approaches learn representations that capture the environment’s transition dynamics via a next-step prediction objective. Some methods learn stochastic models that are aided with image reconstruction [11] or reward-prediction objectives [13]. Other methods combine deterministic forward models with reward prediction and bisimulation metrics [12] or momentum regression targets [23]. Outside of the purpose of representation learning, forward models are used extensively in model-based RL approaches to learn control policies via planning procedures [14, 15, 24, 25].

Stacking several forward models on top of one another forms the levels of a hierarchical model. This type of model has been studied in the context of multiscale temporal inference [26], variational inference [27], and pixel-prediction objectives [28, 29]. Additionally, hierarchical models have been used for speech synthesis [30], learning graph embeddings [31], and decomposing MDPs [32]. Sequence prediction literature has explored the use of hierarchical models via manually-defined connections between levels [29, 33] and using levels with uniform time-step skipping [34, 35].

Unlike the aforementioned forward model approaches, HKSL combines a set of forward models that step in the latent space with independent step sizes without additional prediction objectives. Also, HKSL contains a connection between forward models that learns what to share by using the context from the entire rollout from higher levels and the current timestep of lower levels, which leads to faster learning.

4 Hierarchical k -Step Latent

HKSL’s hierarchical model is comprised of forward models that take steps in the latent space at varying levels of *temporal coarseness*. We define temporal coarseness as the degree to which a level’s forward model skips environment steps. For example, if a forward model predicts the latent representation of a state five steps into the future, it is considered more coarse than a forward model that predicts only one step forward. Coarser levels should learn to attend to information in the environment that takes many steps to manifest in response to an agent’s action. In contrast, finer levels should learn to attend to environmental properties that immediately respond to agent actions. This is because coarser levels need to make fewer predictions to reach steps further into the future than finer levels.

At each learning step, a batch of B trajectories of length k are sampled from the replay memory $\tau = \{(o_t, a_t, \dots, a_{t+k-1}, o_{t+k})_i\}_{i=1}^B$. The initial observation of each trajectory o_t is uniformly randomly sampled on a per-episode basis $t \sim U(1, T - k)^\dagger$. In the following, we will denote the first and last timestep of the batch with $t = 1$ and $t = k$, respectively.

HKSL’s components. See Figure 1 for a visual depiction of the HKSL architecture. HKSL’s hierarchical model is comprised of h levels. Each level l has a forward model f^l , a nonlinear projection module w^l , an online image encoder e_o^l , and a momentum image encoder e_m^l that is updated as an exponential moving average of the online encoder (e.g., [36]). Between consecutive levels there is a communication manager $c^{l,l-1}$ to pass information from one level l to the level below it $l - 1$. The number of steps skipped by a given level n^l is independent of the coarseness of other levels in the hierarchy. Giving each level its own set of learnable models allows specialization to occur at each magnitude of temporal coarseness.

Forward models. HKSL’s forward models are a modified version of the common GRU recurrent cell [37] that allows for multiple data inputs at each step. See Appendix C.3 for a detailed mathematical description. At step $t = 1$, the forward models take the representation produced by the level’s encoder $z_1^l = e_o^l(o_1)$ along with a concatenation of n^l action vectors $\bar{a}_1 = [a_1 | \dots | a_{n^l}]$ to predict the latent representation of a future state $z_{1+n^l}^l = f^l(z_1^l, \bar{a}_1)$. For any following timestep $t > 1$, the forward models take the predicted latent representation z_t^l as input instead of the encoder representation.

Communication managers. Communication managers $c^{l,l-1}$ pass information from coarser to finer levels in the hierarchy ($l \rightarrow l - 1$) while also allowing gradients to flow from finer to coarser levels ($l - 1 \rightarrow l$). A communication manager $c^{l,l-1}$ takes all latent representations produced by level l and one-hot-encoded step t as inputs and extracts information that is relevant for the forward model in level $l - 1$ at step t . For all levels other than the highest level in the hierarchy, the forward models also receive the output of c .

Loss function. HKSL computes a loss value at each timestep within each level in the hierarchy as the normalized ℓ_2 distance between a nonlinear projection of the forward model’s prediction and the “true” latent representation produced by the level’s momentum encoder. Using this “noisy” approximation of the target ensures smooth changes in the target between learning steps and is hypothesized

[†]Ending the range of numbers on $T - k$ guarantees that trajectories do not overlap episodes.

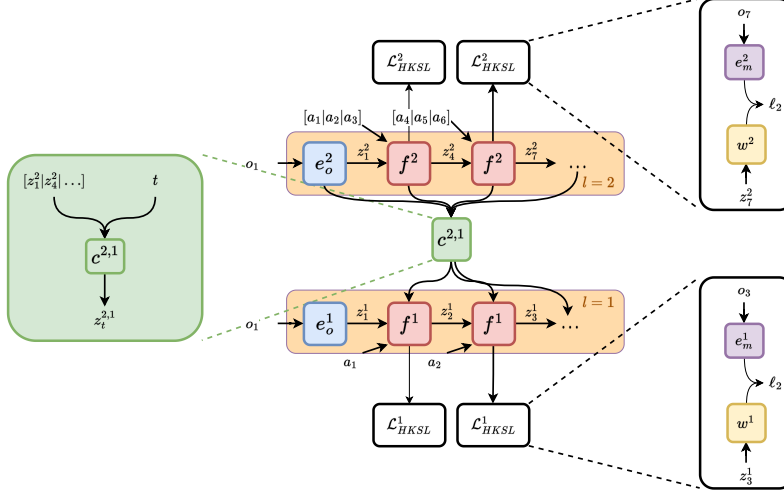


Figure 1: Depiction of HKSL architecture with an “unrolled” two-level hierarchical model where the first level moves at one step $n^1 = 1$ and the second level moves at three steps $n^2 = 3$. First, the online encoders (blue) encode the initial observation o_1 of the sampled trajectory. Next, the forward models (red) predict the latent representations of the following observations, with level 1 predicting single steps ahead conditioned on the level’s previous representation and applied action. The forward model of the second level predicts three steps ahead and receives the previous representation and concatenation of the three applied actions. The communication manager (green) forwards information from the representations of the coarser second level to each forward model step of the first level as additional inputs. All models are trained end-to-end with a normalized ℓ_2 loss of the difference between the projected representations of each level and timestep and the target representations of observations at the predicted timesteps. Target representations are obtained using momentum encoders (purple) and projections are done by the projection model (orange) of the given level.

to reduce the possibility of collapsed representations [38, 39]. We denote the projection model of level l with w^l and the HKSL loss of level l across the minibatch of trajectories τ can be written as

$$\mathcal{L}_{HKSL}^l = \sum_{t=1}^N \mathbb{E}_{a, o \sim \tau} \|w^l (f^l(z_t^l, \bar{a}_t, c^{l+1, l}(\cdot))) - e_m^l(o_{t+n^l})\|_2^2, \quad (1)$$

where N is the number of steps that a given level can take in τ .

HKSL and SAC. We make a few adjustments to the base SAC algorithm to help HKSL fit naturally. For one, we replace the usual critic with an ensemble of h critics. Each critic and target critic in the ensemble receive the latent representations produced by a given level’s encoder and momentum encoder, respectively. We allow critics’ gradients to update their encoders’ weights, and each critic is updated using n -step returns where n corresponds to the n of the level within which the critic’s given encoder resides. By matching encoders and critics in this way, we ensure encoder weights are updated by gradients produced by targets of the same temporal coarseness.

Second, the actor receives a concatenation of the representations produced by all online encoders. HKSL’s actors will make better-informed action selections because they can consider information in the environment that moves at varying levels of temporal coarseness. Finally, we modify the actor’s loss function to use a sum of Q-values from all critics:

$$\mathcal{L}_{actor} = -\mathbb{E}_{a \sim \pi, o \sim \tau} \left[\sum_{l=1}^h Q^l(o, a) - \alpha \log \pi(a | [e_o^1(o) | \dots | e_o^h(o)]) \right]. \quad (2)$$

5 Experiments

We evaluate HKSL with a series of questions and compare it against several relevant baselines. First, is HKSL more sample efficient in terms of agent-environment interactions than other representation

learning methods (§ 5.2)? Second, what is the efficacy of each of HKSL’s components (§ 5.3)? Third, can the levels in HSKL learn to specialize in different magnitudes of temporal coarseness (§ 5.4)? Finally, what does $c^{l,l-1}$ consider when providing information to $l - 1$ from l (§ 5.4)?

5.1 Experimental Setup

Baselines. We use DrQ [9], CURL [7], and PI-SAC [20] as our baselines. DrQ regularizes Q-value learning by averaging temporal difference targets across several augmentations of the same images. CURL uses a contrastive loss similar to CPC [40] to learn image embeddings. PI-SAC uses a Conditional Entropy Bottleneck [41] auxiliary loss with both a forward and backward model to learn a representation of observations that capture the environment’s transition dynamics. All methods use SAC [42, 43] as the base RL algorithm and we use the same encoder, critic, and actor architectures for each agent type to ensure a fair comparison. Additionally, each method uses the same image augmentation. See Appendix C for SAC and HKSL hyperparameters.

Environments. We use six continuous-control environments provided by MuJoCo [44] via the DMControl suite [16, 45], a popular set of environments for testing robotic control algorithms. Each of the six environments uses episodes of length 1k environment steps and a set number of action repeats that controls the number of times the environment is stepped forward with a given action. See Appendix B for further information on the environments.

We use five variations of each environment for a total of 30 tasks. Four of the variations use distractors provided by the Distracting Control Suite API [17], and the fifth variation uses no distractors. We use the “color” and “camera” distractors on both the “easy” and “medium” difficulty settings. The color distractor changes the color of the agent’s pixels on each environment step, and the camera distractor moves the camera in 3D space each environment step. The difficulty setting controls the range of color values and the magnitude of camera movement in each task[†].

5.2 Sample Efficiency

Training and evaluation procedure. In our training scheme, agents are allowed to perform an RL and representation learning gradient update once per action selection. Every 10k environment steps, we perform an evaluation checkpoint, wherein the agent’s policy is sampled deterministically as the mean of the produced action distribution and we collect the mean performance across 10 episodes. All methods are trained with a batch size of 128 for 100k environment steps across five seeds.

Results. We use the “reliable” package [46] to plot statistically robust summary metrics across all 30 tasks in our evaluation suite. Specifically, Figure 2 shows the interquartile mean (IQM) (left) and the optimality gap (middle) along with their 95% confidence intervals (CIs) that are generated via stratified bootstrap sampling[‡] at the 100k steps mark. Optimality gap measures the amount by which a given algorithm fails to achieve a perfect score[†]. Additionally, Figure 2 shows IQM and 95% CIs as a function of environment steps (right). Both of these results show that HKSL significantly outperforms our baselines across our 30 environment testing suite. See Appendix D for individual environment results. We note that simply using a forward model does not guarantee improved performance, as suggested by the comparison between DrQ and PI-SAC.

5.3 Component Ablations

We probe each component of HKSL to determine its contribution to the overall RL policy learning process. Specifically, we test SAC without the hierarchical model but with HKSL’s ensemble of critics (No Repr), HKSL where each level in the hierarchy moves with a single step (All $n = 1$), HKSL without c (No c), HKSL where each level in the hierarchy shares encoders (Shared Encoder), and single-level HKSL ($h = 1$). The No Repr ablation tests whether HKSL’s performance boost is due to the ensemble of critics or the hierarchical model itself. The All $n = 1$ ablation tests our hypothesis that only learning representations at the environment’s presented temporal coarseness can miss out on important information. The No c ablation tests the value of sharing information between

[†]Refer to [17] for details.

[‡]For all plots, we performed at least 5,000 samples.

[†]We note that a perfect score (optimality gap = 0) is technically impossible in the DMControl suite. As such, only the relative positioning of CIs should be considered.

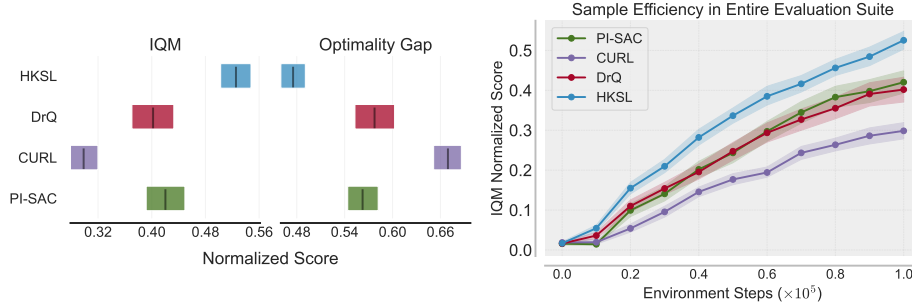


Figure 2: IQM (left) and optimality gap (middle) of evaluation returns at 100k environment steps, and IQM throughout training (right) across all 30 tasks. Shaded areas are 95% confidence intervals.

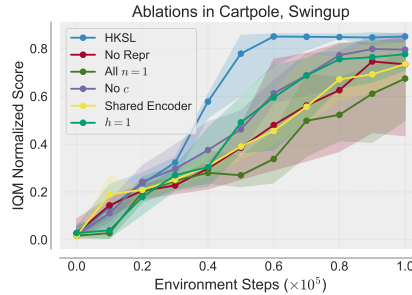


Figure 3: IQM of evaluation returns and 95% CIs for HKSL ablations.

levels. The Shared Encoder ablation tests if level specialization is necessary or if one encoder can learn information at varying temporal coarseness. Finally, the $h = 1$ ablation tests the value of the hierarchy itself by using a standard forward model (e.g., [23, 47]).

See Figure 3 for the performance comparison between these ablations and full HKSL in the no distractors setting of Cartpole, Swingup. All results are reported as IQMs and 95% CIs over five seeds. We highlight that variations without all components perform worse than full HKSL. This suggests that HKSL requires each of the individual components to achieve its full potential.

5.4 Exploring HKSL Specialization and c

Can HKSL’s levels learn to specialize? We hypothesize that one factor leading to HKSL’s sample efficiency is its ability to divide attention to environmental components that move at different speeds. To this end, we test a two-level hierarchical model in Ball in Cup, Catch (BiC) with skips of $n^1 = 1$ and $n^2 = 3$. BiC is an interesting environment for testing our hypothesis because its two core components (the ball and the cup) have significantly different movement characteristics in response to an agent’s action. For example, the agent controls the cup directly, and therefore the effects of an action on the cup manifest immediately. In contrast, the ball is connected to the cup with a soft body (a string), and therefore its response to agent control takes multiple timesteps to manifest. Here, we hypothesize that coarser and finer levels should attend to the ball’s and cup’s dynamics, respectively.

To test our hypothesis, we collect 100 episodes of observations and the corresponding ground-truth locations of the ball and the cup with a random policy. Then, we use the trained encoders of the two-level model to embed the observations and fit a set of linear models to predict the ground-truth locations from the representations. Finally, we step through an episode using the forward models with random actions. We use the trained linear models to predict the location of the ball and cup at every step with the latent representations produced by the forward models. We measure the ℓ_2 distance between the predicted locations and the ground-truth locations. Figure 4 shows the prediction errors for the ball (left) and the cup (right) over 50 episodes. We note that the forward model that moves at a coarser temporal abstraction ($l = 2$) captures the ball’s dynamics more accurately than the forward model that moves at a finer temporal abstraction ($l = 1$). These results suggest that levels can learn to specialize.

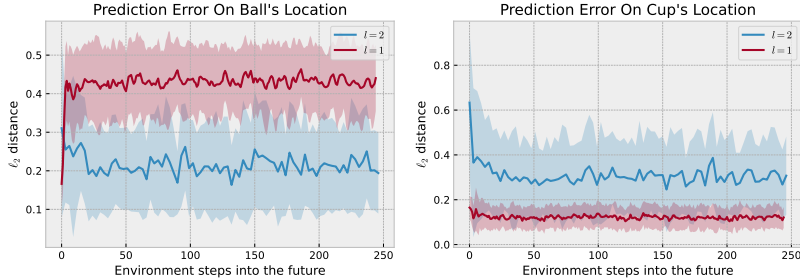


Figure 4: Prediction error of the linear models on the ball’s (left) and the cup’s (right) position. Mean (bold line) \pm one standard deviation (shaded area) over fifty episodes.

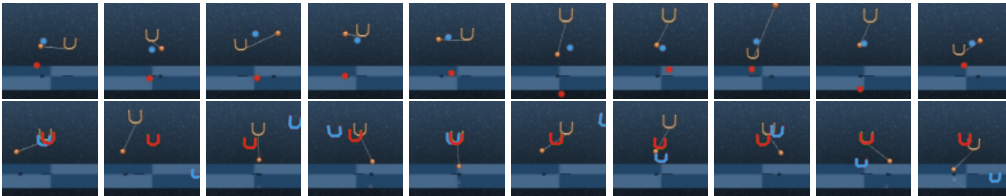


Figure 5: Visualization of the ball-location (top) and cup-location (bottom) predictions from the fitted linear models for $l = 2$ (blue) and $l = 1$ (red) as a function of HKSL’s forward models. The observations occur chronologically left-to-right with skips of 3 environment steps.

Additionally, Figure 5 visualizes the the predicted and ground-truth locations for the ball (top) and cup (bottom) over a trajectory of randomly-chosen actions. These timelines show that $l = 2$ ’s forward model produces representations that capture the ball’s information more precisely than $l = 1$ ’s forward model and vice versa for the cup.

What does c consider? We hypothesize that the communication manager $c^{l,l-1}$ provides a wide diversity of information for f^{l-1} by taking into account the current transition of the below level $l - 1$ as well as the representations from the above level l . To check this hypothesis, we perform two tests. First, we measure the ℓ_2 distance between the vectors produced by c when the step t is changed and other inputs are held fixed. If c completely ignores t , the distance between $c(\cdot, 1)$ and $c(\cdot, 4)$, for example, would be zero. Second, we examine the separability of c ’s outputs on a trajectory-wise basis. If two sampled trajectories are very different, then the representations produced by the above level should change c ’s output such that either trajectory should be clearly separable.

We first train an HKSL agent with two levels in Cartpole, Swingup for 100k environment steps and collect 50 episodes of experiences with a random policy. Then, we randomly sample a trajectory from this collection and step through the latent space with both forward models. We repeat this 100 times, capture c ’s output, and measure the pairwise ℓ_2 distance between every value of t within each sampled trajectory. Figure 6 (left) reports the average distance between each pair. We note that the distance between c ’s output grows as the steps between the pairs grows. This suggests that c considers the transition of the level below it when deciding what information to share. Additionally, we highlight that the distance increases consistently where pairs that are the same number of steps apart are about the same distance apart. For example, pairs (2, 5) and (3, 6) are both three steps apart and share roughly the same average ℓ_2 distance. This suggests that c produces representations that are grouped smoothly in the latent space. Figure 6 (right) visualizes the PCA projections of c ’s outputs from 20 randomly sampled trajectories, where each trajectory is a different color. This figure confirms our second intuition, as the representations are clearly separable on a trajectory-wise basis with representations smoothly varying across steps within the same trajectory.

6 Limitations and Future Work

While HSKL has better sample efficiency than our baselines, its main limitation is that its update steps are computationally expensive. The compute expense is due to the loops over each step in the sampled trajectories and the loops over each level in the hierarchy. This wall-clock-time challenge

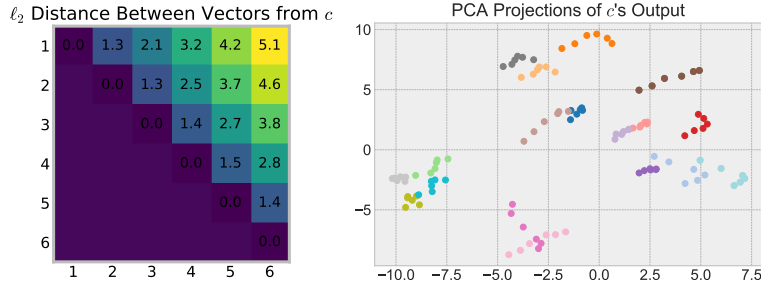


Figure 6: Average distance between vectors produced by c (left). The numbers along the side and bottom correspond to the value of t . PCA projections of representations produced by c for multiple timesteps across 20 trajectories (right) with colors corresponding to trajectories.

makes it difficult to perform an extensive hyperparameter search. See Appendix E for a comparison of compute times between methods. A valuable direction for future research would be to develop methods that automatically identify the most useful magnitudes of temporal coarseness before or during agent-environment interaction.

7 Conclusion

This paper presented Hierarchical k -Step Latent (HKSL), an auxiliary task for accelerating control learning from pixels via a hierarchical latent forward model. Our experiments showed that HKSL’s representations can substantially improve the sample efficiency of downstream RL agents in pixel-based robotic control tasks. We also showed that the temporal coarseness of levels in the hierarchy can lead to specialization on objects whose response to agent actions manifests at different speeds. Finally, we showed that the communication manager organizes information in response to the above and below levels.

References

- [1] D. Kalashnikov, A. Irpan, P. Pastor, J. Ibarz, A. Herzog, E. Jang, D. Quillen, E. Holly, M. Kalakrishnan, V. Vanhoucke, and S. Levine. QT-Opt: Scalable deep reinforcement learning for vision-based robotic manipulation. In *2nd Conference on Robot Learning (CoRL)*, 2018.
- [2] D. Kalashnikov, J. Varley, Y. Chebotar, B. Swanson, R. Jonschkowski, C. Finn, S. Levine, and K. Hausman. Scaling up multi-task robotic reinforcement learning. In *Proceedings of the 5th Conference on Robot Learning (CoRL)*, 2021.
- [3] Y. Lu, K. Hausman, Y. Chebotar, M. Yan, E. Jang, A. Herzog, T. Xiao, A. Irpan, M. Khansari, D. Kalashnikov, and S. Levine. Aw-opt: Learning robotic skills with imitation and reinforcement at scale. In *proceedings of the 5th Conference on Robot Learning (CoRL)*, 2021.
- [4] Y. Chebotar, K. Hausman, Y. Lu, T. Xiao, D. Kalashnikov, J. Varley, A. Irpan, B. Eysenbach, R. C. Julian, and C. F. andyou Sergey Levine. Actionable models: Unsupervised offline reinforcement learning of robotic skills. In *Proceedings of the 38th International Conference on Machine Learning (ICML)*, 2021.
- [5] D. Yarats, A. Zhang, I. Kostrikov, B. Amos, J. Pineau, and R. Fergus. Improving sample efficiency in model-free reinforcement learning from images. *arXiv preprint arXiv:1910.01741*, 2020.
- [6] M. Jaderberg, V. Mnih, W. M. Czarnecki, T. Schaul, J. Z. Leibo, D. Silver, and K. Kavukcuoglu. Reinforcement learning with unsupervised auxiliary tasks. In *International Conference on Learning Representations*, 2017.
- [7] M. Laskin, A. Srinivas, and P. Abbeel. CURL: Contrastive unsupervised representations for reinforcement learning. In *Proceedings of the 37th International Conference on Machine Learning (ICML)*, volume 119, pages 5639–5650, 2020.

- [8] A. Stooke, K. Lee, P. Abbeel, and M. Laskin. Decoupling representation learning from reinforcement learning. In *Proceedings of the 38th International Conference on Machine Learning (ICML)*, volume 139, pages 9870–9879, 2021.
- [9] D. Yarats, I. Kostrikov, and R. Fergus. Image augmentation is all you need: Regularizing deep reinforcement learning from pixels. In *International Conference on Learning Representations (ICLR)*, 2021.
- [10] M. Laskin, K. Lee, A. Stooke, L. Pinto, P. Abbeel, and A. Srinivas. Reinforcement learning with augmented data. In *34th Conference on Neural Information Processing Systems (NeurIPS)*, volume 33, pages 19884–19895, 2020.
- [11] A. X. Lee, A. Nagabandi, P. Abbeel, and S. Levine. Stochastic latent actor-critic: Deep reinforcement learning with a latent variable model. In *Advances in Neural Information Processing Systems (NeurIPS)*, volume 33, pages 741–752, 2020.
- [12] A. Zhang, R. T. McAllister, R. Calandra, Y. Gal, and S. Levine. Learning invariant representations for reinforcement learning without reconstruction. In *International Conference on Learning Representations (ICLR)*, 2021.
- [13] C. Gelada, S. Kumar, J. Buckman, O. Nachum, and M. G. Bellemare. DeepMDP: Learning continuous latent space models for representation learning. In *Proceedings of the 36th International Conference on Machine Learning (ICML)*, 2019.
- [14] D. Hafner, T. Lillicrap, J. Ba, and M. Norouzi. Dream to control: Learning behaviors by latent imagination. In *International Conference on Learning Representations (ICLR)*, 2020.
- [15] D. Hafner, T. Lillicrap, I. Fischer, R. Villegas, D. Ha, H. Lee, and J. Davidson. Learning latent dynamics for planning from pixels. In *International Conference on Machine Learning (ICML)*, pages 2555–2565, 2019.
- [16] Y. Tassa, Y. Doron, A. Muldal, T. Erez, Y. Li, D. de Las Casas, D. Budden, A. Abdolmaleki, J. Merel, A. Lefrancq, T. Lillicrap, and M. Riedmiller. DeepMind control suite. *arXiv preprint arXiv:1801.00690*, 2018.
- [17] A. Stone, O. Ramirez, K. Konolige, and R. Jonschkowski. The distracting control suite – a challenging benchmark for reinforcement learning from pixels. *arXiv preprint arXiv:2101.02722*, 2021.
- [18] R. Bellman. A markovian decision process. *Indiana University Mathematics Journal*, 6:679–684, 1957.
- [19] L. P. Kaelbling, M. L. Littman, and A. R. Cassandra. Planning and acting in partially observable stochastic domains. *Artificial Intelligence*, 101(1):99–134, 1998.
- [20] K.-H. Lee, I. Fischer, A. Liu, Y. Guo, H. Lee, J. Canny, and S. Guadarrama. Predictive information accelerates learning in rl. In *Advances in Neural Information Processing Systems (NeurIPS)*, volume 33, pages 11890–11901, 2020.
- [21] Y. Burda, H. Edwards, D. Pathak, A. Storkey, T. Darrell, and A. A. Efros. Large-scale study of curiosity-driven learning. In *International Conference on Learning Representations (ICLR)*, 2019.
- [22] D. Pathak, P. Agrawal, A. A. Efros, and T. Darrell. Curiosity-driven exploration by self-supervised prediction. In *International Conference on Machine Learning (ICML)*, 2017.
- [23] M. Schwarzer, A. Anand, R. Goel, R. D. Hjelm, A. Courville, and P. Bachman. Data-efficient reinforcement learning with self-predictive representations. In *International Conference on Learning Representations (ICLR)*, 2021.
- [24] D. Ha and J. Schmidhuber. World models. *arXiv preprint arXiv:1803.10122*, 2018.
- [25] M. Zhang, S. Vikram, L. Smith, P. Abbeel, M. J. Johnson, and S. Levine. Solar: Deep structured representations for model-based reinforcement learning. In *International Conference on Machine Learning (ICML)*, 2019.

- [26] J. Schmidhuber. Neural sequence chunkers. Technical report, 1991.
- [27] J. Chung, S. Ahn, and Y. Bengio. Hierarchical multiscale recurrent neural networks. In *International Conference on Learning Representations (ICLR)*, 2017.
- [28] T. Kim, S. Ahn, and Y. Bengio. Variational temporal abstraction. In *33rd Conference on Neural Information Processing Systems (NeurIPS)*, 2019.
- [29] V. Saxena, J. Ba, and D. Hafner. Clockwork variational autoencoders. In *35th Conference on Neural Information Processing Systems (NeurIPS)*, 2021.
- [30] T. Kenter, V. Wan, C.-A. Chan, R. Clark, and J. Vit. CHiVE: Varying prosody in speech synthesis with a linguistically driven dynamic hierarchical conditional variational network. In *Proceedings of the 36th International Conference on Machine Learning (ICML)*, 2019.
- [31] H. Chen, B. Perozzi, Y. Hu, and S. Skiena. Harp: Hierarchical representation learning for networks. In *The Thirty-Second AAAI Conference on Artificial Intelligence (AAAI-18)*, 2018.
- [32] L. Steccanella, S. Totaro, and A. Jonsson. Hierarchical representation learning for markov decision processes. *arXiv preprint: arXiv:2106.01655*, 2021.
- [33] J. Koutnik, K. Greff, F. Gomez, and J. Schmidhuber. A clockwork rnn. In *Proceedings of the 31st International Conference on Machine Learning (ICML)*, 2014.
- [34] M. Kumar, M. Babaeizadeh, D. Erhan, C. Finn, S. Levine, L. Dinh, and D. Kingma. Videoflow: A conditional flow-based model for stochastic video generation. In *International Conference on Learning Representations (ICLR)*, 2020.
- [35] L. Castrejon, N. Ballas, and A. Courville. Improved conditional vrnn for video prediction. In *International Conference on Computer Vision (ICCV)*, 2019.
- [36] K. He, H. Fan, Y. Wu, S. Xie, and R. Girshick. Momentum contrast for unsupervised visual representation learning. In *Proceedings of the IEEE/CVF Conference on Computer Vision and Pattern Recognition (CVPR)*, pages 9726–9735, 2020.
- [37] K. Cho, B. van Merriënboer, D. Bahdanau, and Y. Bengio. On the properties of neural machine translation: Encoder–decoder approaches. In *Proceedings of SSST-8, Eighth Workshop on Syntax, Semantics and Structure in Statistical Translation*, pages 103–111, 2014.
- [38] J.-B. Grill, F. Strub, F. Altché, C. Tallec, P. H. Richemond, E. Buchatskaya, C. Doersch, B. A. Pires, Z. D. Guo, M. G. Azar, B. Piot, K. Kavukcuoglu, R. Munos, and M. Valko. Bootstrap your own latent: A new approach to self-supervised learning. In *34th Conference on Neural Information Processing Systems (NeurIPS)*, 2020.
- [39] A. Tarvainen and H. Valpola. Mean teachers are better role models: Weight-averaged consistency targets improve semi-supervised deep learning results. In *31st Conference on Neural Information Processing Systems (NeurIPS)*, 2017.
- [40] A. van den Oord, Y. Li, and O. Vinyals. Representation learning with contrastive predictive coding. *arXiv preprint arXiv:1807.03748*, 2018.
- [41] I. Fischer. The conditional entropy bottleneck. *Entropy*, 2020.
- [42] T. Haarnoja, A. Zhou, P. Abbeel, and S. Levine. Soft actor-critic: Off-policy maximum entropy deep reinforcement learning with a stochastic actor. In *Proceedings of the 35th International Conference on Machine Learning (ICML)*, volume 80, pages 1861–1870, 2018.
- [43] T. Haarnoja, A. Zhou, K. Hartikainen, G. Tucker, S. Ha, J. Tan, V. Kumar, H. Zhu, A. Gupta, P. Abbeel, and S. Levine. Soft actor-critic algorithms and applications. *arXiv preprint arXiv:1812.05905*, 2018.
- [44] E. Todorov, T. Erez, and Y. Tassa. Mujoco: A physics engine for model-based control. In *2012 IEEE/RSJ International Conference on Intelligent Robots and Systems*, pages 5026–5033, 2012.

- [45] Y. Tassa, S. Tunyasuvunakool, A. Muldal, Y. Doron, S. Liu, S. Bohez, J. Merel, T. Erez, T. Lillicrap, and N. Heess. `dm_control`: Software and tasks for continuous control. *arXiv preprint arXiv:2006.12983*, 2020.
- [46] R. Agarwal, M. Schwarzler, P. S. Castro, A. Courville, and M. G. Bellemare. Deep reinforcement learning at the edge of the statistical precipice. 2021.
- [47] T. McInroe, L. Schäfer, and S. V. Albrecht. Learning temporally-consistent representations for data-efficient reinforcement learning. *arXiv preprint: arXiv:2110.04935*, 2021.
- [48] J. L. Ba, J. R. Kiros, and G. E. Hinton. Layer normalization. *arXiv preprint arXiv:1607.06450*, 2016.
- [49] S. Singh and S. Krishnan. Filter response normalization layer: Eliminating batch dependence in the training of deep neural networks. In *Conference on Computer Vision and Pattern Recognition (CVPR)*, 2020.
- [50] R. Islam, P. Henderson, M. Gomrokchi, and D. Precup. Reproducibility of benchmarked deep reinforcement learning tasks for continuous control. In *Proceedings of the ICML 2017 workshop on Reproducibility in Machine Learning (RML)*, 2017.
- [51] P. Henderson, R. Islam, P. Bachman, J. Pineau, D. Precup, and D. Meger. Deep reinforcement learning that matters. In *Proceedings of The Thirty-Second AAAI Conference on Artificial Intelligence (AAAI-18)*, 2018.

A Extended Background

Soft Actor-Critic. Soft Actor-Critic (SAC) [42, 43] is a popular off-policy, model-free RL algorithm for continuous control. SAC uses a state-action value-function critic Q and target critic \bar{Q} , a stochastic actor π , and a learnable temperature α that weighs between reward and entropy: $\mathbb{E}_{o_t, a_t \sim \pi}[\sum_t \mathcal{R}(o_t, a_t) + \alpha \mathcal{H}(\pi(\cdot|o_t))]$.

SAC’s critic is updated with the squared Bellman error over historical trajectories $\tau = (o_t, a_t, r_t, o_{t+1})$ sampled from a replay memory \mathcal{D} :

$$\mathcal{L}_{critic} = \mathbb{E}_{\tau \sim \mathcal{D}}[(Q(o_t, a_t) - (r_t + \gamma y))^2], \tag{3}$$

where y is computed by sampling the current policy:

$$y = \mathbb{E}_{a' \sim \pi}[\bar{Q}(o_{t+1}, a') - \alpha \log \pi(a'|o_{t+1})]. \tag{4}$$

The target critic \bar{Q} does not receive gradients, but is updated as an exponential moving average (EMA) of Q (e.g., He et al. [36]). SAC’s actor parameterizes a multivariate Gaussian $\mathcal{N}(\mu, \sigma)$ where μ is a vector of means and σ is the diagonal of the covariance matrix. The actor is updated via minimizing :

$$\mathcal{L}_{actor} = -\mathbb{E}_{a \sim \pi, \tau \sim \mathcal{D}}[Q(o_t, a) - \alpha \log \pi(a|o_t)], \tag{5}$$

and α is learned against a static value.

B Environments

Table 1 outlines the action space, the action repeat hyperparameter, and the reward function type of each environment used in this study. The action repeat hyperparameters that are displayed in the table are the standards as defined by [15] and are the same used in most studies in DMControl. The versions of each environment with distractors follow the presented information as well.

Table 1: Dimensions of action spaces, action repeat values, and reward function type for all six environments in the PlaNet benchmark suite.

Environment, Task	$dim(\mathcal{A})$	Action Repeat	Reward Type
Finger, spin	2	2	Dense
Cartpole, swingup	1	8	Dense
Reacher, easy	2	4	Sparse
Cheetah, run	6	4	Dense
Walker, walk	6	2	Dense
Ball in Cup, catch	2	4	Sparse

C Architecture and Hyperparameters

C.1 SAC Settings

All encoders follow the same architecture as defined by [5]. These encoders are made of four convolutional layers separated by ReLU nonlinearities, a linear layer with 50 hidden units, and a final layer norm operation [48]. Each convolutional layer has 32 3×3 kernels and the layers have a stride of 2, 1, 1, and 1, respectively. This in contrast to the encoder used in the PI-SAC study [20], which uses Filter Response Normalization [49] layers between each convolution.

The architectures used by the SAC networks follow the same architecture as deinfed by [5]. Both the actor and critic networks have two layers with 1024 hidden units, separated by ReLU nonlinearities. This is in contrast to the networks used in the PI-SAC study, which uses a different number of hidden units in the actor and critic networks.

Several studies have shown that even small differences in neural network architecture can cause statistically significant differences in performance [50, 51]. As such, we avoid using the original PI-SAC encoder and SAC architectures to ensure a fair study between all methods.

Table 2: SAC Hyperparameters used to produce paper’s main results.

Hyperparameter	Value
Image padding	4 pixels
Initial steps	1000
Stacked frames	3
Evaluation episodes	10
Optimizer	Adam
(β_1, β_2) Optimizer	(0.9, 0.999)
Learning rate	$1e - 3$
Batch size	128
Q function EMA	0.01
Encoder EMA	0.05
Target critic update freq	2
$dim(z)$	50
γ	0.99
Initial α	0.1
Target α	$- \mathcal{A} $
Replay memory capacity	100,000
Actor log stddev bounds	[-10,2]

Table 2 shows the SAC hyperparameters used by all methods in this study. For method-specific hyperparameters (e.g., auxiliary learning rate, architecture of auxiliary networks, etc.), we defaulted to the settings provided by the original authors.

C.2 HKSL Hyperparameters

Table 3 shows the hyperparameters that control HKSL. h represents the number of levels, n contains a list of the skips of each level from lowest to highest level, k shows the length of the trajectory sampled at each training step, learning rate corresponds to the learning rate of all HKSL’s components, and actor update freq corresponds to the number of steps between each actor update. These hyperparameters were found with a brief search over the non-distractor setting of each environment.

HKSL’s communication manager c is a simple two-layer non-linear model. The first layer has 128 hidden units and the second has 50. The two layers are separated by a ReLU nonlinearity.

Table 3: Hyperparameters used for HKSL for each environment.

Environment, Task	h	n	k	Learning rate	Actor Update Freq
Finger, spin	2	[1,3]	3	$1e-4$	2
Cartpole, swingup	2	[1,3]	6	$1e-3$	1
Reacher, easy	2	[1,3]	3	$1e-4$	2
Cheetah, run	2	[4,5]	10	$1e-4$	2
Walker, walk	2	[1,3]	6	$1e-3$	1
Ball in Cup, catch	2	[1,3]	6	$1e-3$	1

C.3 HKSL’s Forward Models

The usual GRU formulation at step t :

$$u_{gru}^t = \sigma(f_{gru}^u([a_t|z_{t-1}])) \tag{6}$$

$$r_{gru}^t = \sigma(f_{gru}^r([a_t|z_{t-1}])) \tag{7}$$

$$h_{gru}^t = \tanh(f_{gru}^h([r_{gru}^t \odot z_{t-1}|a_t])) \tag{8}$$

$$g_{gru}^t = (1 - u_{gru}^t) \odot z_{t-1} + u_{gru}^t \odot h_{gru}^t \tag{9}$$

where each distinct f is an affine transform, σ is the sigmoid nonlinearity, and \odot is the Hadamard product. In order to allow the forward models to take the optional input from c , we

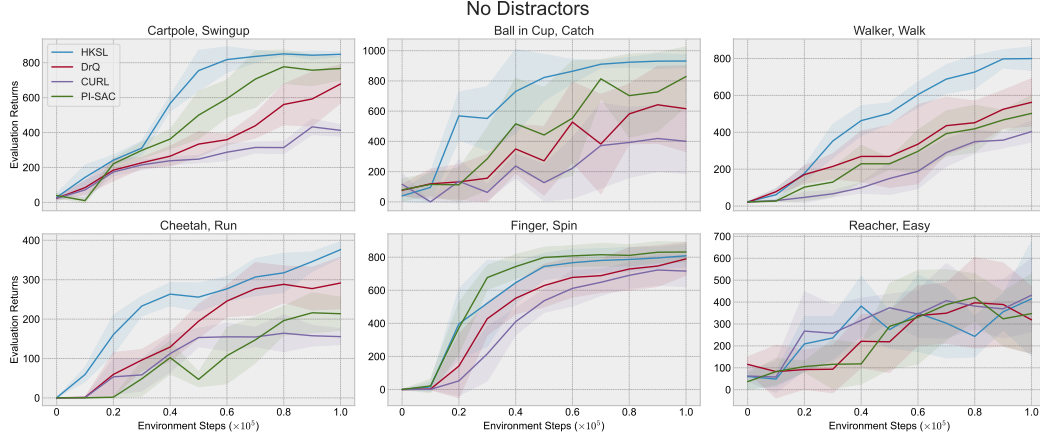


Figure 7: Evaluation returns for agents trained in DMControl without distractors. Bold line depicts the mean and shaded area represents \pm one standard deviation across five seeds.

Table 4: Training time of agent methods, normalized to base SAC.

Method	Normalized Time
SAC	1.0
HKSL	40.0
DrQ	1.8
CURL	1.6
PI-SAC	2.7

add an identical set of additional affine transforms:

$$u_c^t = \sigma(f_c^u([C_t|z_{t-1}])) \quad (10)$$

$$r_c^t = \sigma(f_c^r([C_t|z_{t-1}])) \quad (11)$$

$$h_c^t = \tanh(f_c^h([r_c^t \odot C_t|z_{t-1}])) \quad (12)$$

$$g_c^t = (1 - u_c^t) \odot z_{t-1} + u_c^t \odot h_c^t \quad (13)$$

where C_t denotes the output from c at step t . Finally, the output of the forward model is the average of the two pathways:

$$z_t = \frac{g_c^t + g_{gru}^t}{2} \quad (14)$$

D Individual Environment Results

This section shows the mean (bold lines) \pm one standard deviation (shaded area) for every individual environment and distractor combination. Figure 7 displays the non-distractor environments, Figure 8 shows the color distractors on the easy setting, Figure 9 shows the color distractors on the medium setting, Figure 10 shows the camera distractors on the easy settings, and Figure 11 shows the camera distractors on the medium setting.

E Compute Expense

We measure the wall-clock time required to train the methods used in this paper. To do so, we measure the wall-clock time required to train for 10k environment steps in the no distractor setting of Cartpole, Swingup. Table 4 shows each method normalized to the time of base SAC with no image augmentations. For HKSL’s settings, see Appendix C.2. We note that the value of HKSL’s normalized compute time will change based on its chosen hyperparameters.

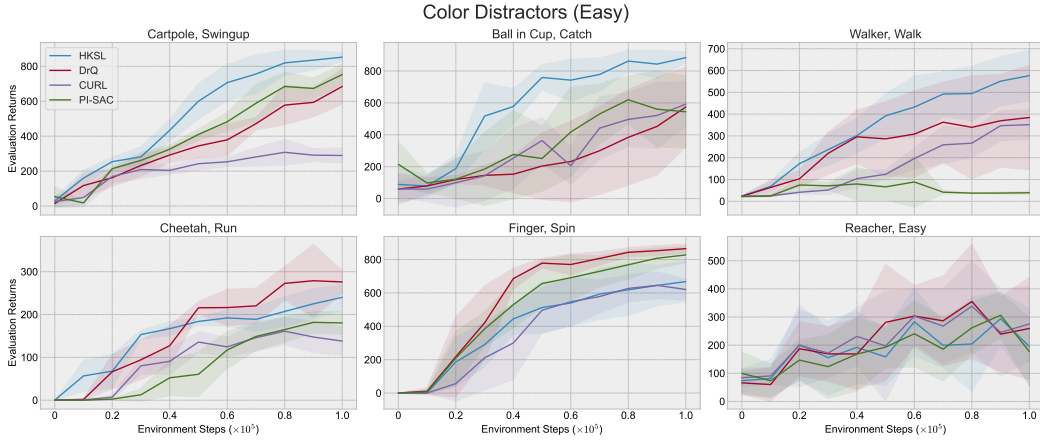


Figure 8: Evaluation returns for agents trained in DMControl with color distractors on the easy setting. Bold line depicts the mean and shaded area represents \pm one standard deviation across five seeds.

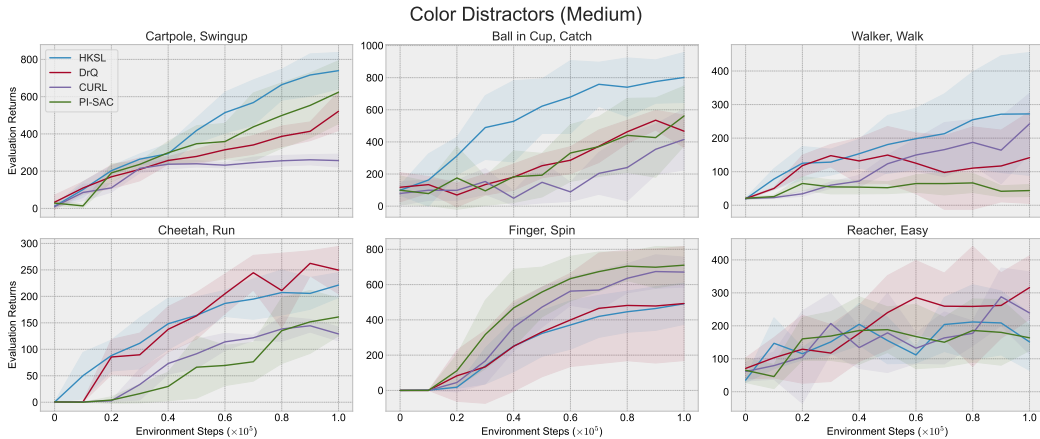


Figure 9: Evaluation returns for agents trained in DMControl with color distractors on the medium setting. Bold line depicts the mean and shaded area represents \pm one standard deviation across five seeds.

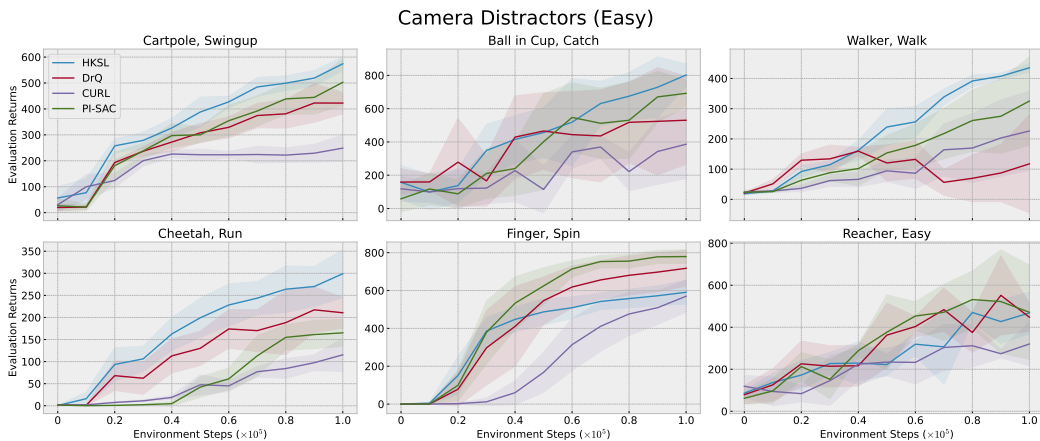


Figure 10: Evaluation returns for agents trained in DMControl with camera distractors on the easy setting. Bold line depicts the mean and shaded area represents \pm one standard deviation across five seeds.

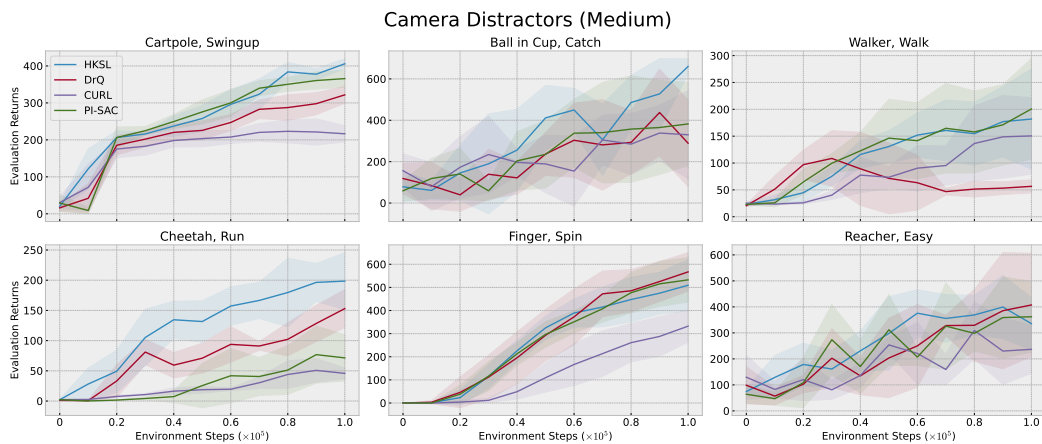


Figure 11: Evaluation returns for agents trained in DMControl with camera distractors on the medium setting. Bold line depicts the mean and shaded area represents \pm one standard deviation across five seeds.